

Seasonal precipitation gradients and their impact on fluvial sediment flux in the Northwest Himalaya

Hendrik Wulf^{a,*}, Bodo Bookhagen^b, Dirk Scherler^c

^a Institut für Geoökologie, Universität Potsdam Karl-Liebknecht-Str. 24, 14476 Potsdam, Germany

^b Department of Geography, 1832 Ellison Hall, University of California at Santa Barbara, Santa Barbara, CA 93106-4060, USA

^c Institut für Geowissenschaften, Universität Potsdam Karl-Liebknecht-Str. 24, 14476 Potsdam, Germany

ARTICLE INFO

Article history:

Received 17 June 2009

Received in revised form 28 November 2009

Accepted 4 December 2009

Available online 8 January 2010

Keywords:

Precipitation

Erosion

Himalaya

Indian Summer Monsoon

Winter westerlies

Suspended sediment

ABSTRACT

Precipitation in the form of rain and snowfall throughout the Himalaya controls river discharge and erosional processes and, thus, has a first-order control on the fluvial sediment flux. Here, we analyze daily precipitation data (1998–2007) of 80 weather stations from the northwestern Himalaya in order to decipher temporal and spatial moisture gradients. In addition, suspended sediment data allow assessment of the impact of precipitation on the fluvial sediment flux for a 10³-km² catchment (Baspa). We find that weather stations located at the mountain front receive ~80% of annual precipitation during summer (May–Oct), whereas stations in the orogenic interior, i.e., leeward of the orographic barrier, receive ~60% of annual precipitation during winter (Nov–Apr). In both regions 4–6 rainstorm days account for ~40% of the summer budgets, while rainstorm magnitude–frequency relations, derived from 40-year precipitation time-series, indicate a higher storm variability in the interior than in the frontal region. This high variability in maximum annual rainstorm days in the orogenic interior is reflected by a high variability in extreme suspended sediment events in the Baspa Valley, which strongly affect annual erosion yields. The two most prominent 5-day-long erosional events account for 50% of the total 5-year suspended sediment flux and coincide with synoptic-scale monsoonal rainstorms. This emphasizes the erosional impact of the Indian Summer Monsoon as the main driving force for erosion processes in the orogenic interior, despite more precipitation falling during the winter season.

© 2009 Elsevier B.V. All rights reserved.

1. Introduction

The spatiotemporal distribution of precipitation in mountain belts is highly complex and difficult to map (Barros and Lettenmaier, 1994; Roe, 2005; Bookhagen and Burbank, 2006), yet a key parameter for erosion processes (Reiners et al., 2003; Bookhagen et al., 2005a). In many studies, the precipitation pattern is invoked as a first-order control on short- and long-term erosion rates (e.g. Thiede et al., 2004; Gabet et al., 2008). However, the complex coupling of precipitation and erosion is difficult to quantify, as precipitation patterns may vary and affect different erosion processes (Bookhagen et al., 2005a). Therefore, it is essential to decipher precipitation gradients and their variations, as these partly govern the efficacy of hillslope processes next to fluvial and glacial dynamics (Gabet et al., 2004; Owen et al., 2005). Unfortunately, reliable high-elevation precipitation data covering several years in the Himalaya remain limited to few locations (Barros et al., 2000; Winiger et al., 2005). In particular, winter

precipitation amounts are largely unknown due to the remoteness and difficult access of high elevations in the orogenic interior (Putkonen, 2004).

Here, we analyze the spatiotemporal distribution of precipitation in the vicinity of the Sutlej Valley in the northwestern Himalaya, based on 80 weather stations (Fig. 1). These stations provide a unique opportunity to investigate climate conditions over several decades and a wide range of elevations (0.4–4.1 km) and topographic settings, i.e., from the wet frontal to the dry interior parts of the orogen. Importantly, the stations cover an area that is influenced by both summer monsoonal and winter westerly precipitation (Lang and Barros, 2004; Bookhagen and Burbank, submitted for publication). This condition allows us to compare the impact of the two contrasting atmospheric circulation regimes on erosion processes, which we observe by responses in suspended sediment load in the Baspa River.

Our analysis addresses three objectives: (1) to quantify precipitation (rainfall and snowfall) gradients in space and time, (2) to analyze the magnitude–frequency relations of rainstorms in different orographic settings, and (3) to relate storm events to erosional processes in the orogenic interior by a case study of river and sediment discharge from the Baspa catchment. Based on these analyses, we are able to test the hypothesis of whether monsoonal rainfall dominates the annual

* Corresponding author. Tel.: +49 331 977 2047; fax: +49 331 977 2068.

E-mail addresses: hendrik.wulf@uni-potsdam.de (H. Wulf), bodo@icess.ucsb.edu (B. Bookhagen), dirk@geo.uni-potsdam.de (D. Scherler).

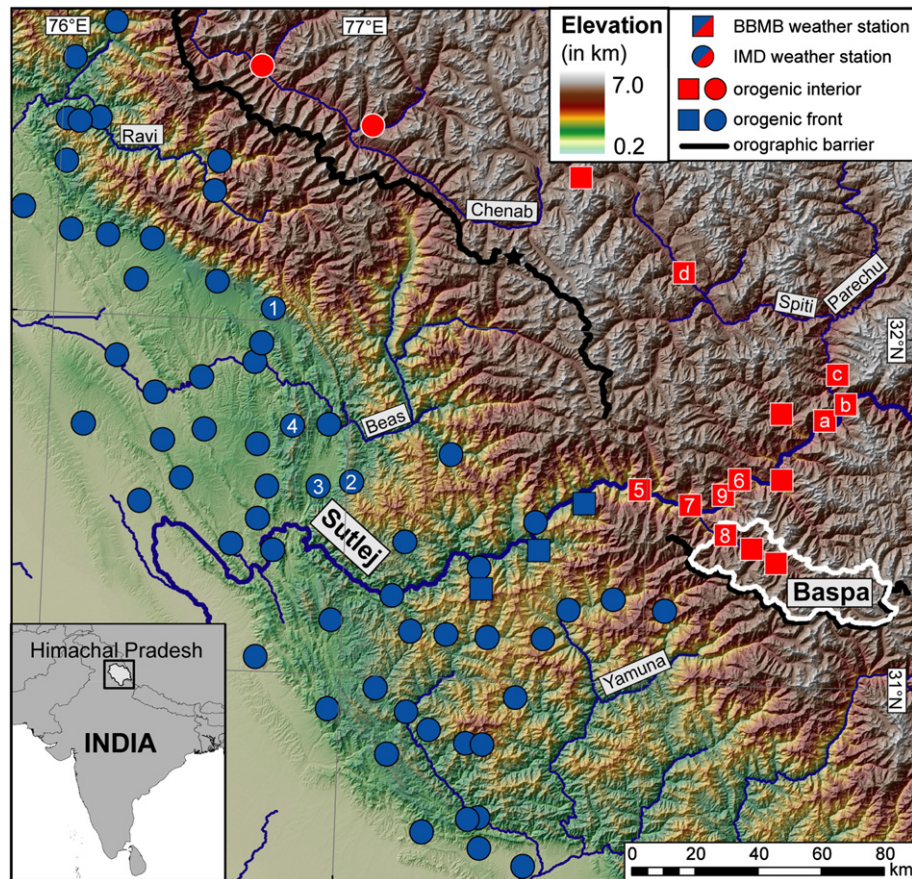


Fig. 1. Shaded-relief and elevation map of northern India (Himachal Pradesh in the Northwest Himalaya). Weather stations represented by blue symbols are situated in the lee of the main orographic barrier (orogenic interior), whereas red symbols indicate stations located to the south of the barrier (orogenic front). Circle- and square-shaped symbols indicate the Indian Meteorological Department (IMD) and the Bhakra Beas Management Board (BBMB), respectively, as operators of these stations. Letters (a–d) and numbers (1–9) refer to weather stations analyzed in Figs. 3 and 5, respectively. Star denotes the snow water equivalent values reported by Wagnon et al. (2007). We point out that the Sutlej River slices through the main orographic barrier and forms a potential conduit for transport of moist air into the orogenic interior. However, the mean summer rainfall recorded by weather stations in this corridor (label 5, 6, 7 and 9) is typically low (0.4–0.2 m), as substantial amounts of the monsoonal moisture are drained at previous orographic barriers. Thus we consider these stations as part of the orogenic interior.

precipitation and fluvial sediment flux budget across the northwestern Himalaya.

2. Precipitation patterns, orographic barriers, and river discharges in the northwestern Himalaya

Precipitation in the northwestern Himalaya is controlled by two atmospheric circulation systems (Gadgil, 2003; Lang and Barros, 2004). First, the Indian Summer Monsoon draws moisture from the Bay of Bengal in the southeast and lasts from June to September. Summer monsoon rainfall amounts decrease from ~1.5 m at the mountain front to ~0.1 m north of the orographic barrier. Rainfall magnitudes vary considerably within short distances as a result of convective, localized monsoonal storms (Barros et al., 2006). Second, the Northern-Hemisphere westerlies supply moisture during December to March, derived from the Mediterranean, Black, and Caspian seas. This winter westerly precipitation is coupled to mid/upper tropospheric, synoptic-scale low-pressure systems, known as Western Disturbances, and is thought to be of stratiform type, i.e., less intense, more prolonged, and encompassing a larger area, than the commonly convective monsoonal rainfall (Putkonen, 2004; Dimri, 2006).

The Himalayan mountain chain forms a pronounced orographic barrier, which separates the southern windward, wet frontal regions from the northern leeward, summer-dry interior parts. This barrier forces moist monsoonal air masses to ascend, which enhances condensation and cloud formation, and ultimately controls the triggering, duration, and intensity of precipitation events (Bookhagen

et al., 2005a). Thus, it typically prevents the migration of moist monsoonal air masses leeward of the orographic barrier and creates an orographic rain shadow in the semi-arid to arid orogenic interior. In our study area the main orographic barrier ranges between 4.0 and 6.6 km in elevation and it coincides with drainage divides of large river systems draining frontal and interior parts of the orogen (Fig. 1). In contrast to the monsoonal air masses, winter westerly moisture is transported at higher tropospheric levels (Weiers, 1995). Thus, the winter westerlies predominantly undergo orographic capture at higher elevations in the orogenic interior, where intense snowfall occurs in areas of high elevation and pronounced relief (Lang and Barros, 2004).

In non-glaciated catchments at the orogenic front, river discharge is closely coupled to summer rainfall, which dominates annual precipitation in these areas (Putkonen, 2004; Craddock et al., 2007). In contrast, within the orogenic interior, snow and glacial melt waters may contribute more than 50% to the annual runoff (Singh and Jain, 2002; Immerzeel et al., 2009; Bookhagen and Burbank, submitted for publication). Thus, in both compartments of the orogen, peak river discharge occurs in summer, although the precipitation timing and spatial gradient of the main moisture-bearing circulation regimes differ fundamentally.

3. Data set and methods

We processed daily precipitation data spanning 10 years (1998–2007) from 80 meteorological stations located within the state of

Himachal Pradesh in NW India (Fig. 1). Snowfall is reported in snow water equivalent (SWE), which has been measured by melting daily snow accumulations. This data-set comprises 63 weather stations from the Indian Meteorological Department (IMD) and 17 high-elevation stations from the Bhakra Beas Management Board (BBMB). At nine stations (Fig. 1: labels 1–9) longer time-series (1961–2007) were available, which we analyzed for summer-rainstorm magnitude–frequency relations. We checked the precipitation data for plausibility according to quality-control measures introduced by Einfalt and Michaelides (2008) and excluded unreliable values from subsequent analyses. Further details on the data location and quality are given in Table A1. The probability density function (PDF) of daily monsoonal rainfall events can be characterized by a gamma distribution (May, 2004). We used the corresponding cumulative density function (CDF) to assess the fraction of total summer rainfall delivered by heavy rainstorms. The magnitude–frequency analysis of maximum summer rainfall days plots the ranked daily rainstorm amounts against their recurrence intervals, which represent the time span between two successive rainfall days of that particular magnitude at that weather station. Gumbel (1958) defined the recurrence interval as:

$$ri = (n + 1) / r \tag{1}$$

where *ri* is the recurrence interval, *n* is the length of the time-series and *r* is the ranking number of the event.

We consider the precipitation during the summer (May–October) as predominantly monsoonal in origin, and precipitation during the winter (November–April) as mainly derived from winter westerlies. In the spatial domain we distinguish between the orogenic interior and front of the mountain range. The orogenic interior is located entirely in the lee (~northeast) of the main orographic barrier and is characterized by high elevations at the river level, i.e., >2 km asl, a high degree of glaciation, low summer precipitation (<0.4 m), and sparse to no vegetation. The orogenic front represents areas that are located southwest of the main orographic barrier and are characterized by high summer rainfall (>0.4 m), various dense vegetation types, and a low degree of glaciation.

To decipher the impact of precipitation on fluvial sediment flux within the orogenic interior, we analyzed daily river discharge and suspended sediment concentration (SSC) from 2004 to 2008 of the Baspa River, the second largest tributary of the Sutlej River. These data were provided by the Baspa-II hydropower station of JayPee Group and sampled at the location of Sangla (Fig. 1: label 8). The SSC values represent the daily average of four filtered and weighed water samples. River discharge is measured once daily, based on a stage-discharge rating curve, which is recalculated each year due to scour-and-fill of the channel bed. We assume a 20% uncertainty in these

data, which arises from (1) changes of the river cross-section caused by scour-and-fill during high discharges and (2) near-shoreline sampling of the SSC data that underestimates the average SSC. To estimate bedload contributions, we analyzed sedimentation rates in the sedimentation reservoir before the water enters the hydropower tunnel. Based on its large initial storage capacity ($1.38 \times 10^{-3} \text{ km}^3$), we assume that the majority of the Baspa bedload flux is captured in the reservoir over a ~500 m-long and 300 m-wide area, about 2 km downstream of Sangla. The sedimentation rates were derived from three depth soundings of the hydropower reservoir in January 2003, October 2004, and April 2007. Flushing of the reservoir took place during a flood from the 5th to 10th of July, which excavated approximately 80% of the reservoir fill (D. P. Goel, Senior General Manager of the Baspa-II hydropower station, personal communication, September 11, 2008). Additional daily SSC measurements downstream of the reservoir allow us to account for accumulation of suspended sediment in the reservoir due to reduced flow velocities. The confidence interval for mean values throughout this study is $\pm 1\sigma$.

4. Results

4.1. Precipitation gradients

At the orogenic front, summer precipitation accounts, on average, for $79 \pm 6\%$ ($0.98 \pm 0.18 \text{ m/summer}$) of the mean annual precipitation (1.23 m/year), while winter precipitation in these low-elevation areas is only $21 \pm 6\%$ ($0.25 \pm 0.07 \text{ m/winter}$). In contrast, the orogenic interior receives on average $42 \pm 14\%$ ($0.27 \pm 0.13 \text{ m/summer}$) of its mean annual precipitation (0.62 m/year) during summer and $58 \pm 14\%$ ($0.35 \pm 0.11 \text{ m/winter}$) during winter (Table 1). These pronounced regional distinctions in precipitation during both seasons are illustrated in more detail by the distribution of mean monthly precipitation (Fig. 2). The most pronounced precipitation gradient occurs during summer, when monsoonal rainfall decreases by more than one order of magnitude within 100 km. Mean summer rainfall magnitudes of up to 2.5 m at high relief sites at the orogenic front decrease sharply to ~0.3 m leeward of the main orographic barrier and reach values of ~0.1 m in the Spiti Valley, 30 km northeast of the orographic barrier (Fig. 1). This negative orogenward precipitation gradient is reversed during winter, when precipitation increases gradually from ~0.2 m over lower elevations (~0.5 km asl) at the orogenic front to ~0.4 m over high elevations (~3 km) in the orogenic interior. As a result, snow water equivalent (SWE) as well as the winter fraction of the annual precipitation increases linearly with elevation (Fig. 3). Weather stations in valley locations within the orogenic interior (Fig. 1: labels a–c), which are shielded by high relief, are less representative, as these are characterized by low mean annual SWE (<0.1 m) irrespective of their elevation (Fig. 3).

Table 1

Ten-year average precipitation and intense precipitation days in the Northwest Himalaya (Himachal Pradesh, India). Only weather stations with a minimum of four continuous years were included in this analysis (orogenic front $n = 41$, interior $n = 10$). We defined storm thresholds for each station by the respective daily precipitation amount of the uppermost 10% of the cumulative distribution function of precipitation (see Fig. 4). Storm days, magnitudes, and percentages represent the seasonal average number of storms exceeding the threshold, their cumulative precipitation, and the percent of average storm magnitudes on the average precipitation magnitude, respectively. The entire cumulative distribution function of summer rainfall and its respective proportion of total summer precipitation are shown in Fig. 4. The given standard deviation ($\pm 1\sigma$) indicates the significant interseasonal variations in precipitation, which are most pronounced in the orogenic interior.

	Precipitation		10% tail of the precipitation probability distribution (storms)			
	Magnitude (mm/season)	Days (#)	storm threshold (mm/day)	Days (#)	Magnitudes (mm/days)	Percentages (%)
<i>Orogenic front</i>						
Summer	977 ± 182	53 ± 6	44 ± 6	6.0 ± 0.6	393 ± 64	40 ± 2
Winter	252 ± 71	20 ± 5	30 ± 6	2.6 ± 0.5	97 ± 27	39 ± 3
<i>Orogenic interior</i>						
Summer	268 ± 128	39 ± 7	16 ± 7	4.6 ± 0.7	121 ± 77	44 ± 7
Winter	354 ± 106	31 ± 6	27 ± 5	3.8 ± 0.8	140 ± 44	40 ± 4

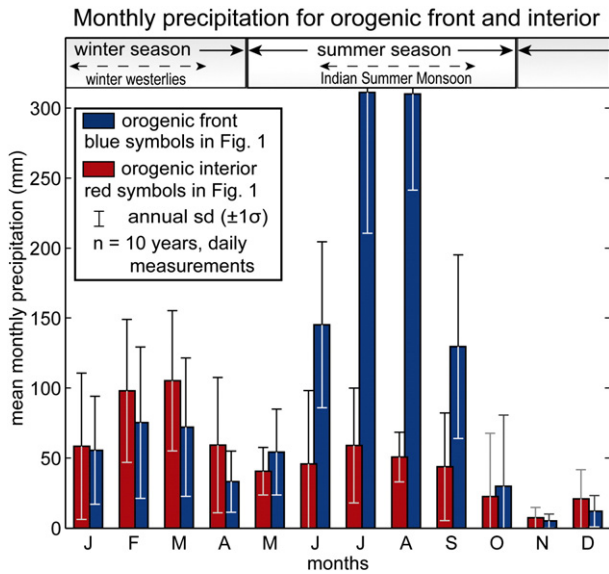


Fig. 2. Average monthly precipitation from 1998 to 2007 of weather stations in the orogenic interior and front. Precipitation during the winter season (November–April) derives predominantly from the winter westerlies, whereas most summer precipitation (May–October) derives from the Indian Summer Monsoon. The error bars represent the annual standard deviation ($\pm 1\sigma$) of the monthly precipitation mean.

4.2. Precipitation intensity and variability

Frequency analyses of the 10-year precipitation data show that during both seasons and in both regions the most intense 10% and 20% of the probability distribution of all precipitation days account for approximately 40% and 60% of the total seasonal precipitation, respectively (Fig. 4). For example, ~40% of the summer rainfall is derived from only 4–6 high-magnitude rainfall days throughout the whole study area (Table 1). Total precipitation during both seasons, in particular within the orogenic interior, is characterized by large interseasonal variations. To verify this regional contrast in summer rainfall variations we analyzed a 40-year precipitation time-series from nine stations in the orogenic interior and at the front (Fig. 1: labels 1–9). In these data we

observe an increase in interseasonal summer-rainstorm variability with elevation. The magnitude–frequency distribution of maximum summer rainfall days reveals that the rate of increase in storm magnitude with respect to return time is higher in the orogenic interior than at the orogenic front (Fig. 5). As a result, the magnitude of a 2-year rainstorm is 3.8 times smaller in the interior region than compared to the frontal region, whereas the 20-year rainstorm is only 1.9 times smaller. Furthermore, 10-year peak rainstorms in the orogenic interior are comparable in strength to annual peak rainstorms at the orogenic front.

4.3. Case study: Rainfall and erosion in the Baspa Valley

The Baspa River is the second largest tributary of the Sutlej (Fig. 1). Its 1102-km² catchment is situated in the orogenic interior and glaciers cover 20% of the catchment area. Based on the Shuttle Radar Topographic Mission (SRTM) Version 2 topographic data with a 90-m grid-cell size, the hillslopes of the Baspa valley are on average 27° steep and basin elevations range from 1.8 to 6.4 km. Three valley-weather stations in Sangla (2.7 km asl), Rakchham (3.1 km), and Chhitkul (3.4 km) indicate 0.31 ± 0.06 m mean summer precipitation and 0.37 ± 0.13 m mean winter precipitation. Throughout the year, precipitation increases with elevation at a rate of ~0.12 m/km. River discharge and suspended sediment concentrations start to rise in April/May due to snow and glacier melt, and peak in July/August due to additional monsoonal rainfall. Low-flow conditions are regained by mid- to late October. Due to low river transport capacities and suspended sediment concentrations during winter, more than 99% of the fluvial sediment transport takes place during summer (Table 2).

Daily SSC correlate by a power-law with daily river discharge (Q) as described by the sediment rating curve (Campbell and Bauder, 1940): $SSC [g l^{-1}] = 3.8 \times 10^{-4} [g l^{-1} s m^{-3}] \times Q^{1.6} [m^3 s^{-1}]$, $r^2 = 0.77$ (Fig. 6). This correlation suggests increased reworking of sediment storage in the riverbed as the river discharge increases. A clockwise hysteresis loop in the suspended sediment flux is weakly pronounced and indicates slightly more suspended sediment transport on the rising limb of the hydrograph (May, June) than on the falling limb (September, October) for a given discharge. Within the 5-year SSC record we identified eight peak events with anomalously high suspended sediment concentrations ($SSC > 2 g l^{-1}$), which are

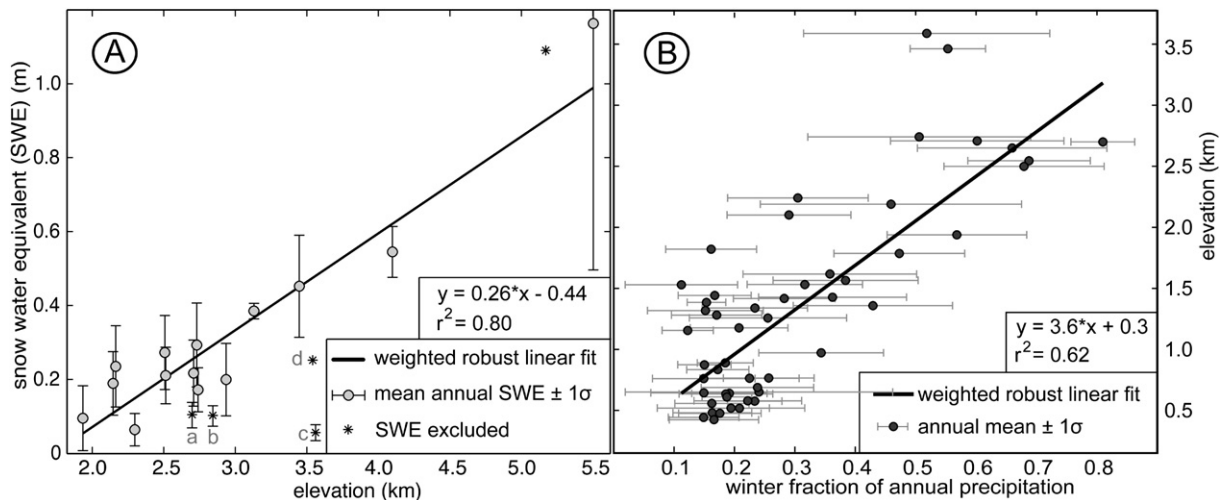


Fig. 3. (A): Relation of snow water equivalent (SWE) and elevation. Annually measured minimum SWE values above 5 km are taken from Wagnon et al. (2007). Due to high annual variations we excluded data from two locations with less than three continuous years (d of Fig. 1), as well as three orographically shielded valley stations (a–c of Fig. 1) at the Sutlej–Spiti confluence which are characterized by unrepresentative low annual precipitation. These three stations (a–c of Fig. 1) affect the regression by a reduced coefficient of determination ($r^2 = 0.65$) with the following linear model: $y = 0.24 * x - 0.42$. (B): Fraction of winter precipitation on annual precipitation vs. elevation. We excluded data from stations with less than four continuous years to account for high annual variations. The robust linear fit implies an increasing dominance of winter precipitation in high elevations. In both figures the robust correlation was weighted by the number of measurement years and error bars reflect $\pm 1\sigma$.

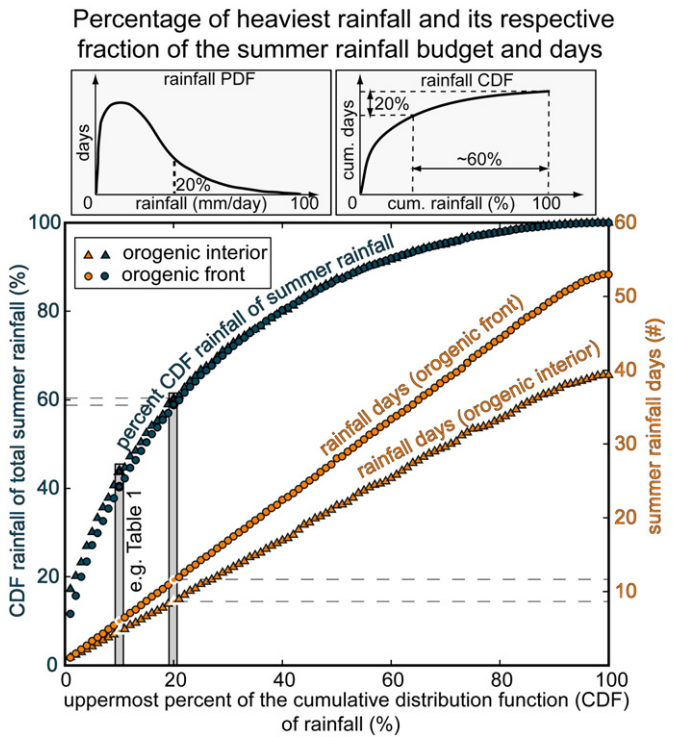


Fig. 4. Percentage of the cumulative distribution function of summer rainfall, its respective proportion of total summer precipitation, and the rainfall days, which account for these fractions in the orogenic interior and the orogenic front. Two sketches on the gamma probability density function (PDF) of summer rainfall and the corresponding cumulative distribution function (CDF) illustrate the derivation of the x- and y-variables using the example of the 20% heaviest rainfall days, which account for approximately 60% of the total summer precipitation. In both regions, only a few rainfall days account for large proportions of the summer precipitation budget. Precise numbers for the case of the 10% heaviest precipitation days are given in Table 1.

characterized by large residuals from the sediment rating curve. These eight peak SSC events lasted for 1–5 days and occurred almost exclusively during June to August (Fig. 7). In total, they account for 62% (3×10^6 t) of the total 5-year suspended sediment load. The two most prominent of these eight events (starting 5th July 2005 and 11th August 2007) coincided with several day-long and extensive monsoonal rainstorms and account for 50% (2.4×10^6 t) of the total 5-year suspended sediment load. Maximum daily rainfall in the Baspa Valley during these two events (1st and 7th events in Fig. 7) amounted to 54 mm and 35 mm, respectively. Based on the magnitude–frequency relation of maximum summer rainstorms in the orogenic interior, such daily rainstorms re-occur at intervals of 3 to 5 years (Fig. 5). Additional analyses of all 80 weather stations in Himachal Pradesh reveal that these two storms were characterized by a large spatial extent (>100 km), lasted 2–3 days in most records, and migrated from the orogenic front across the main orographic barrier into the orogenic interior. The 10-year record indicates that 17 such rainstorms occurred at the orogenic front, but only ten reached the orogenic interior.

An example of the hillslope processes that took place during the first event, starting on 5th July 2005, is a 2.5×10^5 -m³ landslide, which occurred 4 km downstream of Sangla (Fig. 1: label 8) and is therefore not included in our SSC data. On 5th July 2005 the rainstorm magnitude in Sangla culminated with 41 mm day⁻¹ and triggered slope failure along a 0.5 km reach (Fig. 8). The landslide eroded parts of a fan, which was covered by sparse vegetation and subject to previous slope failures, as indicated by its morphology. The only road to Sangla and into upstream villages crossed this landslide area and was subsequently cut off. Access to the Baspa Valley was inhibited for 3 months (Sandhu, 2005; Sharma, 2006).

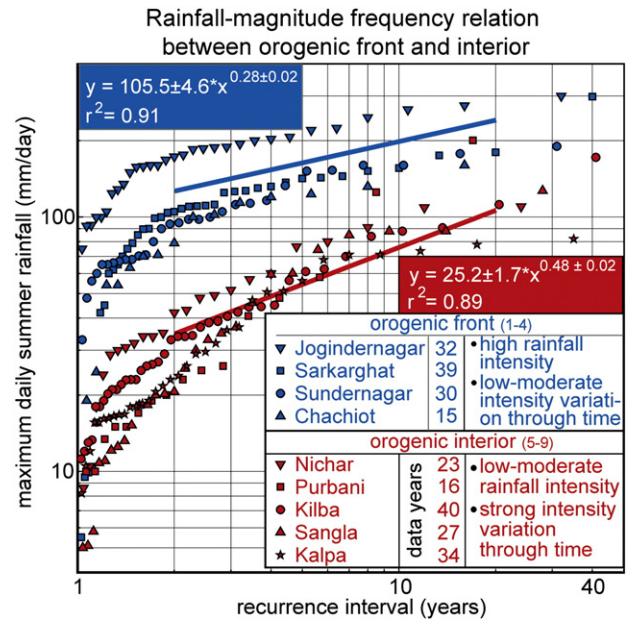


Fig. 5. Maximum daily summer precipitation at the orogenic front (open symbols, 1–4) and at the orogenic interior (filled symbols, 5–9), see Fig. 1 for locations. Data cover the period 1961–2007; years with missing data were excluded. The trend lines represent a power-law fit to all data within a recurrence interval of 2 to 20 years in both spatial regions. The coefficient of determination (r^2) represents the mean fit of individual station correlations within each region. The orogenic interior shows a steeper increase in recurrence interval with respect to rainfall rate that indicates a higher intensity variation of rainstorms as compared to the orogenic front.

We estimate modern erosion rates in the Baspa Valley by accounting for suspended sediment load (SSL) and bedload flux. The average erosion rate derived from suspended sediment load, E_{SSL} , is calculated according to

$$E_{SSL} = (\rho \times A)^{-1} \times \sum_i (SSC_i \times Q_i) \quad (2)$$

where SSC_i is the mean daily suspended sediment concentration, Q_i is the daily Baspa river discharge, ρ is the density of the suspended sediment (1.4 t m^{-3}), and A is the drainage area (989 km^2) of the Sangla sub-catchment. We estimate bedload contributions based on reservoir sedimentation rates of the hydropower plant within the Baspa valley (Table 3). The two periods analyzed (1st period: Jan 2003 to Oct 2004; 2nd period: Oct 2004 to Apr 2007) exhibit large differences, which are mostly related to the occurrence of high SSC events during the second period. For example, during the flood in June 2005 the high SSC increased the daily SSL by a factor of 19.3, whereas river discharge, which controls the quantity of bedload transport, increased only by a factor of 1.3. Thus, high SSC events increase the SSL several times more than bedload, which consequently increases the SSL–bedload-ratio. Since high SSC events occurred frequently from 2005 onwards, we assume that the approximate 2:1 SSL–bedload-ratio of the second period is a reliable estimate for the entire 5-year SSL time-series (2004–2008). The average modern erosion rate of the Baspa River based on SSL and bedload from 2004 to 2008 is $1.05 \pm 0.8 \text{ m year}^{-1}$ (Table 2). The pronounced variability relates in large part to the occurrence of peak SSC events, which vary strongly in magnitude. For example, the two most prominent peak events (1st and 7th events in Fig. 7) account for 61% and 77% of the high annual SSL in 2005 and 2007, which translate into 0.67 mm/5 days and 1.09 mm/4 days erosion rates, respectively (Table 2).

Table 2

Annual suspended sediment load, runoff, and erosion rates of the Baspa catchment from 2004 to 2008. Suspended sediment load during summer accounts for >99% of the annual budget. Peak SSC events, as shown in Fig. 7, account for large fractions of the annual suspended sediment load budget and high erosion rates. Annual runoff reflects variations in annual precipitation and temperatures. Annual erosion rates, which account for suspended sediment load and bedload, vary significantly due to varying magnitudes of peak SSC events.

Year	Suspended sediment load (SSL)					Runoff Annual m/year	Modern erosion rate		
	Annual	Summer	Summer/annual	Peak SSL/annual	Peak SSL erosion		SSL	Bedload (2:1 ratio)	Combined load
	10^5 t	10^5 t	%	%	mm/events		mm/year	mm/year	mm/year
2004	2.06	2.05	99.6	0.0	0.00	0.83	0.15	0.07	0.22
2005	15.27	15.24	99.8	63.0	0.67	1.37	1.10	0.55	1.65
2006	5.12	5.07	99.0	35.6	0.13	1.24	0.37	0.18	0.55
2007	19.60	19.56	99.8	81.3	1.15	1.07	1.42	0.71	2.12
2008	6.22	6.21	99.7	48.2	0.21	0.92	0.45	0.22	0.67
Mean	9.65	9.62	99.6	45.6	0.43	1.09	0.70	0.35	1.05
Std	7.43	7.42	0.3	30.7	0.47	0.22	0.54	0.27	0.80

5. Discussion

Our analysis shows that the spatially and temporally varying moisture fluxes have very different effects on the hydrologic and erosional regime of the Baspa Valley. In the high-elevation areas of the orogenic interior, winter snowfall is higher than summer rainfall and thus leads to significant glacial accumulation. Studies by Bookhagen and Burbank (submitted for publication) and Singh and Jain (2002) show that snow and ice melt during summer contribute significantly (>50%) to river discharge in the Sutlej Valley but high-magnitude/low-frequency monsoonal rainstorms dominate our historic short-term records of fluvial sediment flux. Similar observations on extreme events have been made in other semi-arid to arid mountainous environments (Wolman and Miller, 1960; Coppus and Imeson, 2002). The rare occurrence of these events in the orogenic interior implies that reliable estimates of mean erosion rates derived from SSC data need to be based on longer observation periods as compared to the orogenic front (cf. Gabet et al., 2008).

In frontal regions, intense monsoonal rainfall accounts for vigorous fluvial incision and mass wasting on an annual basis (e.g. Gabet et al., 2004; Craddock et al., 2007; Burtin et al., in review). The large spatial

extent (>100 km) and duration (>2 days) of the two intense rainstorm events that triggered vast sediment discharges in the Baspa Valley is characteristic for synoptic-scale rainstorms, which intrude far into the interior of the orogen and are, therefore, different from typically more localized convective rainfall events (Barros et al., 2004). We argue that such extensive rainstorms are able to mobilize large amounts of sediment material in the orogenic interior, which is characterized by steep vegetation-free hillslopes and numerous bare alluvial fans that provide readily erodible sediment sources. Indeed, a study by Bookhagen et al. (2005a) shows that during an abnormally strong rainfall year in 2002, erosion on non-vegetated hillslopes mostly occurred through debris flows.

We found that maximum annual rainstorm events in the orogenic interior exhibit strong variations in rainfall intensity (Fig. 5). This implies that peak erosional events, which are linked to heavy rainstorm events, also undergo large variations, as reflected by the large deviations in annual suspended sediment flux (Table 2). Precipitation data from the central Himalaya, suggest similar differences in the variability of monsoonal storm intensity between the orogenic interior and the orogenic front (Craddock et al., 2007). This regional contrast in monsoonal storm variability between frontal and interior regions throughout the Himalaya is presumably related to the main orographic barrier. In a similar setting further west in the Karakoram, rare occurrences of summer monsoon rainfall far behind the main orographic barrier have been associated by Weiers (1995) to the coincidence of monsoonal depressions with southerly air flows at the 500 hPa level. This synoptic configuration during summer is given when troughs in the upper tropospheric westerly jet are located above the Hindu Kush–Pamir region and divert the westerlies southwards (Weiers, 1995). However, the interaction of westerly airflow and monsoonal depressions, which leads to large annual variations in rainstorm magnitude, is restricted to the western end of the Himalaya.

Slope failure induced by significant monsoonal rainstorms is a common phenomenon in the orogenic interior, as documented by Bookhagen et al. (2005a) and witnessed by the authors in the years 2002, 2005, 2007 and 2009. Based on these observations, we deduce that heavy monsoonal rainfalls triggered two of the eight peak SSC events and infer that these were linked with hillslope processes as shown in Fig. 8. During the remaining six peak SSC events the recorded daily rainfall amounts in the Baspa Valley were moderate to low (Fig. 7) and no earthquakes occurred in the region. It is likely that rainfall amounts in the valley locations underestimate the rainfall at higher elevations and that convective monsoonal rainstorms vary considerably in intensity within short distances (Barros et al., 2006). Antecedent moisture may also increase the regolith field capacity such that moderate rainfall amounts produce positive pore pressures, which reduce slope stabilities (Gabet et al., 2004). Alternatively, transiently stored sediments in the riverbed could have been remobilized due to increased discharge by snow and glacial melt.

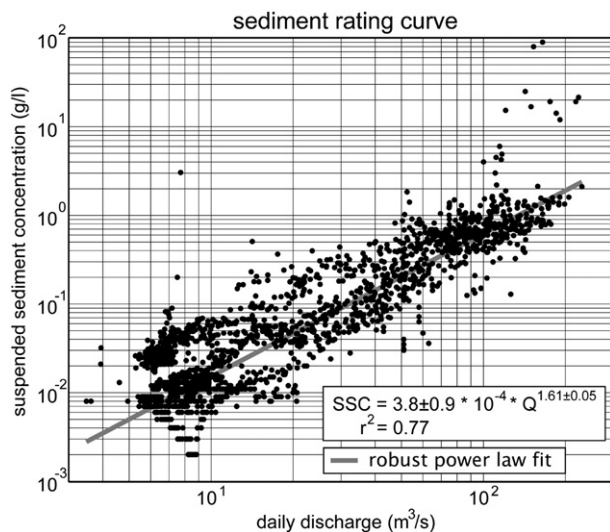


Fig. 6. Sediment rating curve of the Baspa River showing suspended sediment concentration (SSC) as a function of daily river discharge (Q). Events with anomalously high SSC values (>2 g l⁻¹) are analyzed further and shown in Fig. 7. SSC variance is typically of the order of two magnitudes for a given discharge level due to annually varying sediment availability, seasonal hysteresis effects, and sudden sediment delivery events caused by landslides, snow avalanches or glacial sediment discharges. Note that the rating curve underestimates sediment flux as it does not capture the peak SSC events adequately. The power-law fit is based on the least square method.

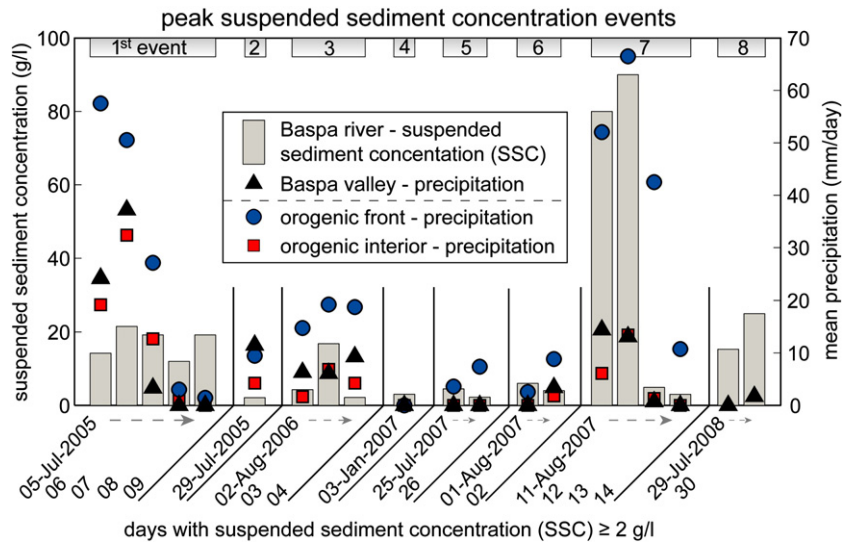


Fig. 7. Days with suspended sediment concentration (SSC) $\geq 2 \text{ g l}^{-1}$ in the Baspa River. Daily rainfall represents the mean of three stations in the Baspa Valley, 17 in the orogenic interior, and 63 at the orogenic front. Note the coincidence of heavy precipitation, lasting for 2–3 days, and the two most significant SSC events (1st and 7th events).

Most notably here is the effect of rain-on-snow, which results in rapidly rising river discharges that occasionally reach flood levels (Singh et al., 1997; McCabe et al., 2007). In addition, Gabet et al. (2008) also found a dependence of high sediment flux on high temperatures during the absence of rainfall in July and August and suggest a sub-glacial origin as a potential sediment source.

Our modern erosion rate estimates, based on SSL and bedload data, reflect the erosion of fluvial sediment storage and possibly include sediments from hillslope erosion, which is suggested by the rapid increase in SSC levels of more than one magnitude during the two major rainstorm events. This modern erosion rate does not necessarily reflect the average catchment-wide erosion, as the river could be in a stage of aggradation or incision and thus under- or over-represent the amount of erosion. Furthermore, we acknowledge that our estimated bedload rates, which were derived from reservoir sedimentation rates, contain interpolated SSL data and missing bedload flux due to the reservoir flushing during the flood in July 2005. However, the bedload component of the sedimentary flux in Alpine rivers is typically difficult to measure (Leopold and Emmett, 1976). Given the scarce bedload data from the Himalaya, we rely on these locally derived estimates. The applied 2:1 SSL–bedload–ratio is also consistent with mapped lacustrine (SSL) and deltaic (bedload) deposits from a mid-Holocene landslide-dammed lake in the upper Marsyandi

catchment, a similar environment in the central Himalaya (Pratt-Sitaula et al., 2007). Nevertheless, this ratio might underestimate the real bedload, as Galy and France-Lanord (2001) suggest that bedload fluxes in the Himalayas may be of the same magnitude as suspended sediment fluxes. If this were the case for the Baspa Valley, the modern erosion rate increases by 33% to $\sim 1.4 \text{ mm year}^{-1}$.

Gabet et al. (2008) analyzed modern mean erosion rates from individual catchments in the Marsyandi Valley in the central Himalaya, which range from 0.1 ± 0.1 to $2.0 \pm 0.6 \text{ mm year}^{-1}$, and found an increase in modern erosion rates with increasing average monsoonal rainfall amounts. Tributary catchments from the Marsyandi region, which are comparable to the Baspa Valley, show lower mean erosion rates ($0.5 \pm 0.3 \text{ mm year}^{-1}$), as those catchments are characterized by less annual runoff and moderate magnitudes of peak SSC events (Gabet et al., 2008). To evaluate the impact of monsoonal precipitation on erosion rates within a 10^4 -year time-scale, we compare our modern estimate ($1.05 \pm 0.8 \text{ mm year}^{-1}$) with Holocene erosion yields in the context of varying monsoonal strength. Volumetric analyses of lake sediments behind an early to mid-Holocene landslide deposit in the Baspa Valley indicate upstream erosion yields of $4.3 \pm 0.4 \text{ mm year}^{-1}$, about four times higher than present-day average yields (Bookhagen et al., 2005b). This period was characterized by intensified monsoon rainfalls and highlights the

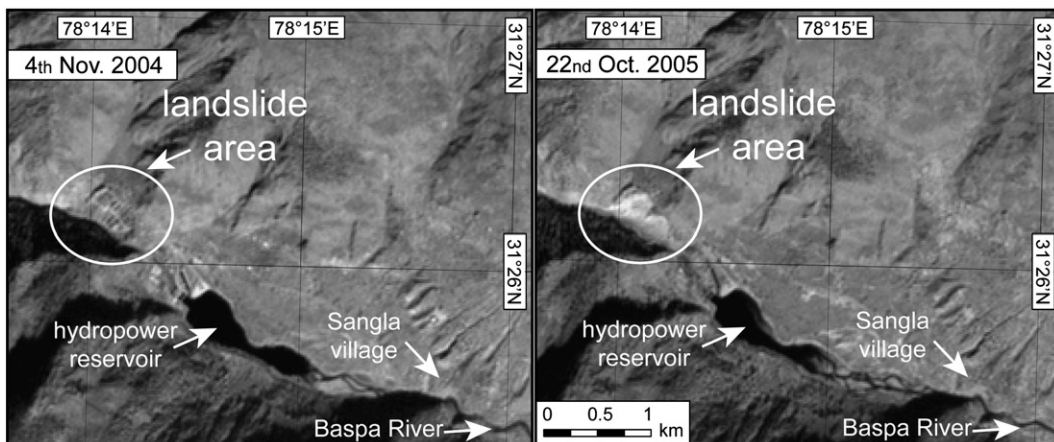


Fig. 8. Landslide area in the Baspa Valley 4 km downstream of Sangla shown by Advanced Spaceborne Thermal Emission Reflection Radiometer (ASTER) images before and after the event (5th July 2005).

Table 3
 Estimation of the Baspa River bedload. The reservoir sedimentation volumes were derived from depth soundings. We converted these volumes into mass by assuming a reservoir fill bulk density of 2 t m^{-3} . On average, 14% of suspended sediment load influx during summer accumulates in the reservoir due to reduced flow velocities. The suspended sediment–bedload-ratio differs considerably, which is in large part due to peak SSC events that occurred during the second period. We consider both SSL–bedload ratios as end members of a possible range. It is likely that the SSL during the first period would further increase, due to increased river discharge following pronounced snowfall during the winter 2002/03 (0.5 m SWE in Chhitkul at 3.4 km asl). During the second period, the bedload component is underestimated, as bedload was not captured during the flood in July 2005.

Period	Reservoir accumulation	Reservoir accumulation	Reservoir SSL	Reservoir bedload	River SSL	SSL/bedload	Bedload/combined load
	10^5 m^3	10^5 t	10^5 t	10^5 t	10^5 t	Ratio	%
Jan 2003–Oct 2004	7.2	14.4	0.8	13.6	5.8 ^a	1:2.3	70
Oct 2004–Apr 2007	5.3 ^b	10.6	1.5	9.0 ^c	20.4	2.3:1	31

^a SSL was not recorded between Jan–Jul 2003 and is replaced by an average SSL amount from 2004–2008 (excluding all peak SSC events during that period).

^b We accounted for an estimated reservoir–fill excavation of 80% (personal communication, D.P. Goel) due to reservoir flushing during the flood from 5th to 10th July 2005.

^c Bedload flux during the flood (5th–10th July 2005) is not included.

susceptibility of semi-arid regions behind the orographic barrier to millennial-scale monsoonal strength variations.

6. Conclusions

Precipitation data from 80 weather stations from the western Himalaya reveal that summer precipitation from May to October accounts for ~80% of the mean annual precipitation at the orogenic front, whereas winter precipitation from November to April accounts for ~60% of the annual budget in the orogenic interior. Although 40% of summer precipitation falls during 4–6 rainstorm events in both regions, rainstorm intensity in the orogenic interior varies considerably more than at the orogenic front. Analysis of a 40-year time-series indicates that on average, peak rainfall magnitudes vary significantly more between years in the orogenic interior than at the front. Not surprisingly, these rainstorm events have a large impact on sediment flux: during a 5-year period the two highest suspended sediment load (SSL) events lasted a total of nine days and accounted for ~50% of the total suspended sediment flux of the Baspa Valley. These high SSL events coincide with extensive, synoptic-scale rainstorms that last on average for 2–3 days. Such peak erosional events, which re-occur at intervals of 3 to 5 years, account for large variations of modern erosion rates in the Baspa Valley ($1.05 \pm 0.8 \text{ mm year}^{-1}$). Thus, despite the great importance of winter westerly-derived moisture for glaciers and river discharge in the orogenic interior, sporadic heavy monsoonal rainstorms dominate the fluvial sediment flux.

Acknowledgments

This research was funded by the German Research Council (DFG, Deutsche Forschungsgemeinschaft) graduate school GK-1364. H.W. acknowledges M.R. Strecker for financial support while visiting UCSB. We thank the employees of BBMB, IMD and JayPee Group, who provided their data on weather records, river discharge and suspended sediment concentration for us. We are grateful to Tashi Longpo, Swami Ray, Bishan Lal, Clara Chrzanowski, and Juliane Hirte for the valuable support during the fieldwork. We thank O. Korup and an anonymous reviewer for their thoughtful and constructive reviews.

Appendix A. Supplementary data

Supplementary data associated with this article can be found, in the online version, at doi:10.1016/j.geomorph.2009.12.003.

References

Barros, A.P., Lettenmaier, D.P., 1994. Dynamic modeling of orographically induced precipitation. *Reviews of Geophysics* 32, 265–284.
 Barros, A.P., Joshi, M., Putkonen, J., Burbank, D.W., 2000. A study of 1999 monsoon rainfall in a mountainous region in central Nepal using TRMM products and rain gauge observations. *Geophysical Research Letters* 27, 3683–3686.

Barros, A.P., Kim, G., Williams, E., Nesbitt, S.W., 2004. Probing orographic controls in the Himalayas during the monsoon using satellite imagery. *Natural Hazards and Earth System Sciences* 4, 29–51.
 Barros, A.P., Chiao, S., Lang, T.J., Burbank, D., Putkonen, J., 2006. From weather to climate – seasonal and interannual variability of storms and implications for erosion processes in the Himalaya. *GSA Special Paper* 398, 17–38.
 Bookhagen, B., Burbank, D.W., 2006. Topography, relief, and TRMM-derived rainfall variations along the Himalaya. *Geophysical Research Letters* 33, L08405. doi:10.1029/2006GL026944.
 Bookhagen, B., Burbank, D.W., Towards a complete Himalayan hydrologic budget: The spatiotemporal distribution of snowmelt and rainfall and their impact on river discharge. submitted to *Journal of Geophysical Research-Earth Surface*.
 Bookhagen, B., Thiede, R.C., Strecker, M.R., 2005a. Abnormal monsoon years and their control on erosion and sediment flux in the high, arid northwest Himalaya. *Earth and Planetary Science Letters* 231, 131–146.
 Bookhagen, B., Thiede, R.C., Strecker, M.R., 2005b. Late Quaternary intensified monsoon phases control landscape evolution in the northwest Himalaya. *Geology* 33, 149–152.
 Burtin, A., Bollinger, L., Cattin, R., Vergne, J., Nabelek, J.L., in review. Spatiotemporal Sequence of Himalayan Debris Flow from High-Frequency Seismic Noise Analysis. accepted to *Journal of Geophysical Research - Earth Surface*.
 Campbell, F.B., Bauder, H.A., 1940. A rating-curve method for determining silt-discharge of streams. *EOS (Transactions - American Geophysical Union)* 21, 603–607.
 Coppus, R., Imeson, A.C., 2002. Extreme events controlling erosion and sediment transport in a semi-arid sub-Andean valley. *Earth Surface Processes and Landforms* 27, 1365–1375.
 Craddock, W.H., Burbank, D.W., Bookhagen, B., Gabet, E.J., 2007. Bedrock channel geometry along an orographic rainfall gradient in the upper Marsyandi River valley in central Nepal. *Journal of Geophysical Research-Earth Surface* 112, F03007. doi:10.1029/2006JF000589.
 Dimri, A., 2006. Surface and upper air fields during extreme winter precipitation over the western Himalayas. *Pure and Applied Geophysics* 163, 1679–1698.
 Einfalt, T., Michaelides, S., 2008. Quality control of precipitation data. *Precipitation: Advances in Measurement, Estimation and Prediction*, pp. 101–126.
 Gabet, E.J., Burbank, D.W., Putkonen, J.K., Pratt-Sitaula, B.A., Ojha, T., 2004. Rainfall thresholds for landsliding in the Himalayas of Nepal. *Geomorphology* 63, 131–143.
 Gabet, E.J., Burbank, D.W., Pratt-Sitaula, B., Putkonen, J., Bookhagen, B., 2008. Modern erosion rates in the High Himalayas of Nepal. *Earth and Planetary Science Letters* 267, 482–494.
 Gadgil, S., 2003. The Indian monsoon and its variability. *Annual Review of Earth and Planetary Sciences* 31, 429–467.
 Galy, A., France-Lanord, C., 2001. Higher erosion rates in the Himalaya: geochemical constraints on riverine fluxes. *Geology* 29, 23–26.
 Gumbel, E.J., 1958. *Statistics of Extremes*. Columbia University Press, New York.
 Immerzeel, W.W., Droogers, P., de Jong, S.M., Bierkens, M.F.P., 2009. Large-scale monitoring of snow cover and runoff simulation in Himalayan river basins using remote sensing. *Remote Sensing of Environment* 113, 40–49.
 Lang, T.J., Barros, A.P., 2004. Winter storms in the central Himalayas. *Journal of the Meteorological Society of Japan* 82, 829–844.
 Leopold, L.B., Emmett, W.W., 1976. Bedload measurements, East Fork River, Wyoming. *Proceedings of the National Academy of Sciences of the United States of America* 73, 1000–1004.
 May, W., 2004. Variability and extremes of daily rainfall during the Indian summer monsoon in the period 1901–1989. *Global and Planetary Change* 44, 83–105.
 McCabe, G.J., Clark, M.P., Hay, L.E., 2007. Rain-on-snow events in the western United States. *Bulletin of the American Meteorological Society* 88, 319–328.
 Owen, L.A., Finkel, R.C., Barnard, P.L., Ma, H., Asahi, K., Caffee, M.W., Derbyshire, E., 2005. Climatic and topographic controls on the style and timing of Late Quaternary glaciation throughout Tibet and the Himalaya defined by Be-10 cosmogenic radionuclide surface exposure dating. *Quaternary Science Reviews* 24, 1391–1411.
 Pratt-Sitaula, B., Garde, M., Burbank, D., Oskin, M., Heimsath, A., Gabet, E., 2007. Bedload-to-suspended load ratio and rapid bedrock incision from Himalayan landslide-dam lake record. *Quaternary Research* 68, 111–120.
 Putkonen, J.K., 2004. Continuous snow and rain data at 500 to 4400 m altitude near Annapurna, Nepal, 1999–2001. *Arctic, Antarctic, and Alpine Research* 36, 244–248.
 Reiners, P.W., Ehlers, T.A., Mitchell, S.G., Montgomery, D.R., 2003. Coupled spatial variations in precipitation and long-term erosion rates across the Washington Cascades. *Nature* 426, 645–647.

- Roe, G.H., 2005. Orographic precipitation. *Annual Review of Earth and Planetary Sciences* 33, 645–671.
- Sandhu, K., 2005. Sangla valley still cut off, *The Tribune*. <http://www.tribuneindia.com/2005/20050910/himachal.htm#4>, Chandigarh, India.
- Sharma, D.D., 2006. Floods and Flash Floods in Himachal Pradesh: A Geographical Analysis, <http://nidm.gov.in/idmc/Proceedings/Flood/B2-%206.pdf>.
- Singh, P., Jain, S.K., 2002. Snow and glacier melt in the Satluj River at Bhakra Dam in the western Himalayan region. *Hydrological Sciences Journal-Journal des Sciences Hydrologiques* 47, 93–106.
- Singh, P., Spitzbart, G., Hubl, H., Weinmeister, H.W., 1997. Hydrological response of snowpack under rain-on-snow events: a field study. *Journal of Hydrology* 202, 1–20.
- Thiede, R.C., Bookhagen, B., Arrowsmith, J.R., Sobel, E.R., Strecker, M.R., 2004. Climatic control on rapid exhumation along the Southern Himalayan Front. *Earth and Planetary Science Letters* 222, 791–806.
- Wagnon, P., Rajesh, K., Arnaud, Y., Linda, A., Sharma, P., Vincent, C., Pottakal, J., Berthier, E., Ramanathan, A., Hasnain, S.I., Chevallier, P., 2007. Four years of mass balance on Chhota Shigri Glacier, Himachal Pradesh, India, a new benchmark glacier in the western Himalaya. *Journal of Glaciology* 53, 603–611.
- Weiers, S., 1995. Zur Klimatologie des NW-Karakorum und angrenzender Gebiete. Statistische Analysen unter Einbeziehung von Wettersatellitenbildern und eines Geographischen Informationssystems (GIS): *Bonner geographische Abhandlungen*, vol. 92, pp. 1–169.
- Winiger, M., Gumpert, M., Yamout, H., 2005. Karakorum–Hindukush–western Himalaya: assessing high-altitude water resources. *Hydrological Processes* 19, 2329–2338.
- Wolman, M.G., Miller, J.P., 1960. Magnitude and frequency of forces in geomorphic processes. *Journal of Geology* 68, 54–74.